

# Position Optimization of the Roberts – Chebyshev Cognate – Compliant Mechanisms

**Dušan Stojiljković, Nenad T. Pavlović and Nenad D. Pavlović**

Faculty of Mechanical Engineering, University of Niš

A. Medvedeva 14, 18000 Niš, Serbia; e-mail: dusan.stojiljkovic@masfak.ni.ac.rs,  
nenad.t.pavlovic@masfak.ni.ac.rs, nenad.d.pavlovic@masfak.ni.ac.rs

---

*Abstract: Instead of relying solely on moving rigid-body joints, compliant mechanisms motion is defined, thanks to their joints' relative flexibility, i.e., flexure hinges. As alternatives to the rigid-body Roberts-Chebyshev mechanism, which allows the coupler point to be directed along a roughly rectilinear route, two compliant cognate mechanisms have been devised in this study. Guaranteeing the same input-output coupler tracing point, these cognate mechanisms have different link lengths but come from the same kinematic chain. For each of the two examples of newly built cognate-compliant mechanisms, the "coupler" point's guiding accuracy on the rectilinear trace (minimum divergence between the exact rectilinear and realized trace) and the mobility have been computed. Due to the need for comparison, newly obtained compliant mechanisms are often designed with flexure hinges of already widely known shapes. Hence, the cognate-compliant mechanisms with notch joints (circular flexure hinges) have first been analyzed. The introduction of undercut flexure hinges in the compliant structure and the use of position optimization tools have improved the performance of the cognate-compliant mechanism with better guidance accuracy and greater mobility.*

*Keywords: Compliant mechanisms; Flexure hinges; Cognate-compliant mechanisms; Roberts–Chebyshev mechanism; Positional optimization*

---

## 1 Introduction

While functionality is the most fundamental request for any engineering solution, the optimality of the solution is another request that has gained tremendous importance over the previous decades. Such a request fits well into the general request for the sustainability of resources and energy. The optimality criteria of an engineering solution depend on numerous aspects, such as the application field of the developed solution, demanded service life, available time, tools for development, etc. Hence, the engineers try to provide innovative ways of improving their solutions based on various criteria. Focusing on mechanisms, a wide range of developments are aimed at this objective. Those include analysis

and optimization of the working space of mechanisms [1-3], design and topology optimization of mechanisms concerning the applied production techniques [4-7], as well as application of innovative, lightweight materials [8-10].

Instead of relying solely on rigid-body joints, the relative flexibility of compliant mechanisms' joints contributes to some of their mobility. Using flexure hinges (in the literature can be found also as compliant joints) in the mechanism construction has various benefits, including the ability to build a mechanism as a single part, a reduction in weight, no need for lubrication, and the elimination of wear, clearance, friction, and noises. They are therefore appropriate for use in micromachining. Because of its advantages in robotics, medical technology, sensor application, and handling compressible items, compliant mechanisms and actuators are becoming more and more important [11] [12]. On the other hand, the mobility, or ability to realize relatively minor displacements, of the mechanisms with flexure hinges is constrained.

Numerous studies cover both the structure and purpose of flexure hinges and compliant mechanisms. For the components of compliant mechanisms, several authors have defined fundamental terminology and classification [13-15]. It has also been suggested to compare the design method of a compliant mechanism class with a small flexible section and comparatively inflexible sections of the mechanism [14] [16]. Ananthasuresh and Kota [17] have presented the homogenization method as a formal structural optimization technique for designing flexible structures. Based on the novel ideas of technically feasible joints from nature, Böttcher et al. [18] proposed motion-task elastically mobile structures for positioning and manipulation in engineering.

The impact of the flexure hinges' geometry and material type on the accuracy of some of their guiding points has been examined by Pavlović et al. [19-22].

The initial compliant mechanism concept for axial link translation was presented by Pavlović and Pavlović [23].

The guiding precision of cognate-compliant mechanisms based on Watt's linkage has been examined by Pavlović and Stojiljković [24].

Yuan et al. [25] have established the rigid-flexible coupling virtual prototyping model of the excavator attachment to develop the dynamic performance of the intelligent excavating process.

There are many papers confirming the fact that the results obtained by Finite Element Analysis (FEA) are similar to the results obtained by other numerical procedures or experimentally, meaning that the results obtained by FEA can be successfully used for the displacement analysis of compliant mechanisms [26-31].

Hao et al. [32], have presented the conceptual design of compliant translational joints (CTJs) via three approaches: the parallelogram-based method, the straight-line motion mechanism-based method, and the combination-based method. New

CTJs are proposed using three approaches, including an asymmetric double parallelogram mechanism with slaving mechanisms, several compact and symmetric double parallelogram mechanisms with slaving mechanisms, a general CTJ using the center drift compensation, a CTJ using Robert's linkage, and several combination designs.

Compliant mechanisms are usually designed using two techniques: the kinematics approach and the structural optimization approach. In this paper, the kinematics approach has been used, that is, a compliant mechanism has been designed as the rigid-body linkage's opposite, which is capable of realizing the intended function (rigid-body replacement method). The rigid-body Roberts-Chebyshev (R-Ch) mechanism has a basic and two cognate-compliant analogs that allow the coupler point to be guided along a roughly rectilinear route. Hence, designing these three cognate-compliant four-bar linkages is the subject of this paper.

The research seeks to identify the mobility restrictions of the recently introduced cognate-compliant mechanisms (CCM) to facilitate the process of designing the compliant mechanisms.

The goals of this paper, the applied methods and materials as well as its contributions that highlight its novelty are as follows:

- This paper has introduced the design of the cognate-compliant four-bar linkages. The two CCMs have been developed as counterparts of the rigid-body R-Ch mechanism, where the coupler point can be directed on an approximate rectilinear trace. The guiding accuracy, that is, the difference between realized and exact rectilinear trace, as well as the mobility, that is, determining the constraint position of the links, have been analyzed and compared for all above-mentioned CCMs being suitable to realize approximate rectilinear guiding of the coupler point.
- The position analysis of the compliant mechanisms was performed using the ANSYS software. It has been assumed that the compliant mechanisms are made of material piacryl with the specific properties regarding Young's modulus, flexural strength and the thickness of material. A characteristic ANSYS element type PLANE 183 (2-D 8-Node Structural Solid) has been used to perform the calculation for rectangular cross-sectional area elements
- The position optimization and newly introduced undercut flexure hinges have improved the performance of the CCM with better guidance accuracy and greater mobility.

## 2 The R-Ch Rigid-Body Four-Bar Linkage

The R-Ch four-bar linkage's parameters (link lengths, position of input crank  $\varphi$ ), permit accomplishing a horizontal movement  $\Delta x_C = 5$  mm of the coupler point C, with the smallest possible deviation from the perfect rectilinear trace ( $\Delta y_C$ ), have been demonstrated by Pavlović [19]. Each coupler curve, produced by a four-bar linkage with four revolute joints, can be generated by three different four-bar linkages, one basic and two cognate linkages (Roberts-Chebyshev theorem). Fig. 1 shows basic (presented with black color) and two cognate R-Ch rigid-body four-bar linkages:  $A_0A_1CB_1K_0$  and  $B_0B_2CA_2K_0$  (presented with grey and green color retrospective), where the coupler point C remains in the coupler's corner as a ternary link, which can also be directed along an approximation of the rectilinear trace (presented with red dotted line).

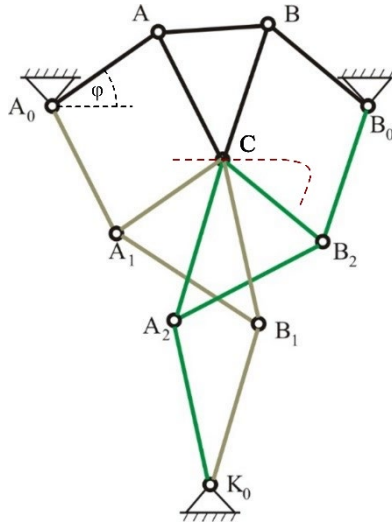


Figure 1

The constructions of cognate R-Ch four-bar linkages from the basic R-Ch four-bar linkage

The links position of the cognate R-Ch rigid-body four-bar linkages have been determined by using the following relations:

$$\overline{A_0A_1} \parallel \overline{AC} \wedge \overline{B_0B_2} \parallel \overline{BC} \quad (2a)$$

$$\Delta A_1CB_1 \sim \Delta ABC \wedge \Delta B_2CA_2 \sim \Delta ABC \quad (2b)$$

$$\overline{A_2K_0} \parallel \overline{B_1C} \wedge \overline{B_1K_0} \parallel \overline{A_2C} \Rightarrow \Delta A_0B_0K_0 \sim \Delta ABC \quad (2c)$$

### 3 The R-Ch Cognate-Compliant Mechanisms with Circular Flexure Hinges

A notch joint or circular flexure hinge (Fig. 2) is one of the characteristic types of flexure hinges [19]. This flexure hinge's planar geometry is entirely determined by two variables: the relatively rigid segments' width  $w_R$  and the relatively elastic segments' width  $w_E$  (Fig. 2a). Point 1 is the cross point of two symmetry axes of the circular flexure hinge (Fig. 2b) corresponding to revolute joint of the rigid-body counterpart. The other characteristic key points of a notch joint (Fig. 2a) can be calculated by using the set of equations defined in [23].

A Roberts-Chebyshev cognate-compliant mechanisms (R-ChCCMs) with circular flexure hinges (Fig. 3a and 3c) were created based on the cognate R-Ch rigid-body four-bar linkages (Fig. 3b and 3d) by connection of the previously defined characteristic key points into the lines. The lines define specific areas. The areas have been afterward transformed to the set of nodes.

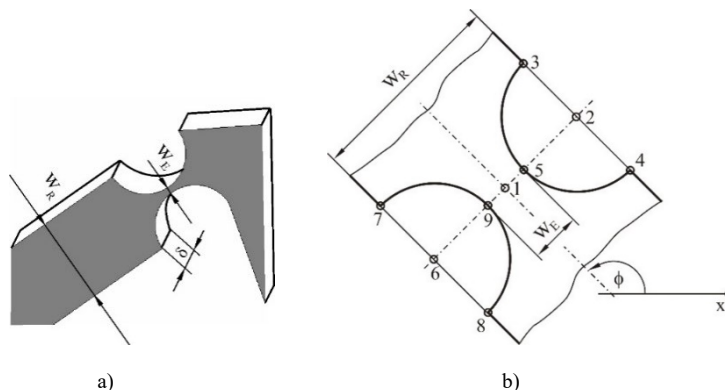


Figure 2

A circular flexure hinge (notch joint)

The rigid-body input crank  $A_0A$  is coincident with one of the symmetry axes of the flexure hinges  $A_0$  and  $A$ , whereas the rigid-body follower  $B_0B$  is coincident with one of the symmetry axes of the flexure hinges  $B_0$  and  $B$ . The input crank value of  $\varphi = 37^\circ$  defines the symmetrical position of the mechanisms with the smallest difference between realized and exact rectilinear trace, at which  $\overline{AB} \parallel \overline{A_0B_0}$  (Fig. 1). Therefore, we choose the starting input crank value of  $\varphi = 35^\circ$  (motion range  $\varphi = 35^\circ \div 40^\circ$ ). The middle of the "input crank" ( $F_a$ ) or the middle of the "follower" ( $F_b$ ) are two examples of input load force acting sites that have been studied.

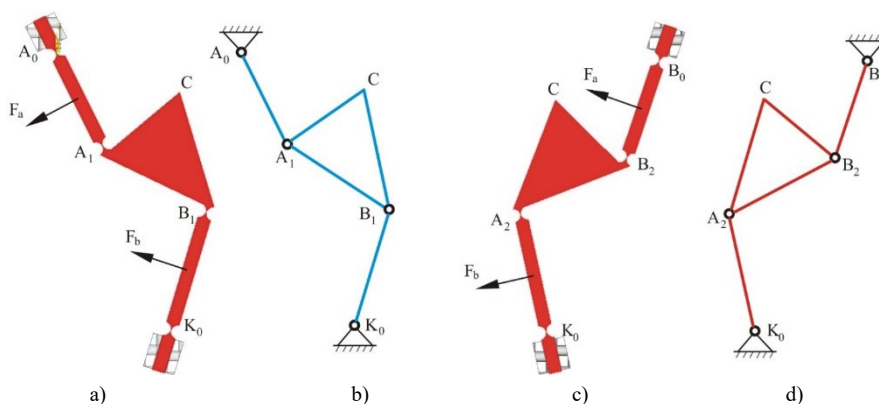


Figure 3

The first R-ChCCM with circular flexure hinges (a) and its rigid-body counterpart  $A_0A_1CB_1K_0$  (b)  
 The second R-ChCCM with circular flexure hinges (c) and its rigid-body counterpart  $B_0B_2CA_2K_0$  (d)

## 4 The R-ChCCM's Guiding Accuracy and Mobility

We have analyzed the "coupler" point guiding accuracy (on the rectilinear trace of  $\Delta x_C = 5$  mm) of the CCMs with circular flexure hinges. The values of the following flexure hinge parameters have been assumed: relatively rigid segments width  $w_R = 10$  mm and relatively elastic segments width  $w_E = 1$  mm.

The FEA of the CCMs was performed using the ANSYS software. It has been assumed that the CCMs are made of material piacryl with the properties: Young's modulus  $E = 3700$  N/mm<sup>2</sup>, flexural strength  $\sigma_{bs} = 90$  N/mm<sup>2</sup>, the thickness of material  $\delta = 4$  mm. A characteristic ANSYS element type PLANE 183 (2-D 8-Node Structural Solid) has been used to perform the calculation for rectangular cross-sectional area elements. The guiding accuracies were compared for two different cases of the location of the point of application of input load force: in the middle of the "input crank" -  $F_a$  and in the middle of the "follower" -  $F_b$  (Fig. 3a and 3c). This is because the input load force application point does not necessarily have to be located on the compliant mechanism's "input crank" only. The results have been shown in Table 1 [33].

Table 1  
 Guiding accuracy of the R-ChCCMs

Guiding inaccuracy $\Delta y_C$ [ $\mu\text{m}$ ]		
R-ChCCM	Input force case $F_a$	Input force case $F_b$
First cognate (Fig. 3a)	0.9 ( $F_a=2.86$ N)	2.9 ( $F_b=5$ N)
Second cognate (Fig. 3c)	4.4 ( $F_a=2.64$ N)	3.3 ( $F_b=3.62$ N)

The first R-ChCCMs with the point of application of input load force situated in the middle of the "input crank" have provided the highest guiding accuracy (minimum variation between absolute rectilinear and realized trace) of the "coupler" point on the rectilinear trace.

First, an experimental analysis of the flexural strength of a sample of the link with a circular flexure hinge manufactured by pyacryl (Fig. 4) was conducted [34]. We have loaded the sample at the point W with the different weight mass  $m$  (different gravity force  $F = mg$  acting perpendicular to the sample), that is, with the different bending moment  $M = mga$ , where  $a$  is the length of the sample. The vertical displacement of the point W ( $\Delta y_w$ ) has been measured by an inductive displacement transducer.

The paper [36] also dealt with the experimental research of the displacement of the compliant four-bar linkages for rectilinear guiding. The input motion has been caused by micrometer screw, providing the input force perpendicular to the member. The measuring results have corresponded to the results obtained by ANSYS Software, so it has been concluded that this software can be used in displacement calculation purposes of the compliant mechanisms.

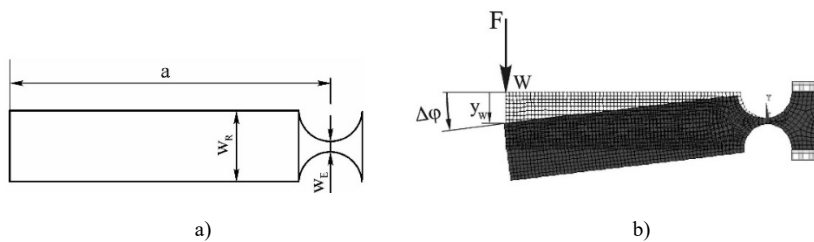


Figure 4

A link with compliant circular flexure hinges in the undeformed and deformed position

The ability to utilize ANSYS Software in the displacement and stress calculation of links with flexure hinges and compliant mechanisms in the elastic area of the flexural strain ( $\sigma_{\max} = 0$  to  $65 \text{ N/mm}^2$ ) is demonstrated by the comparison of experimentally and numerically obtained data as well as in the hyper-elastic area of the flexural strain ( $\sigma_{\max} = 65$  to  $90 \text{ N/mm}^2$ ) [34].

For the values  $\sigma_{\max} > 90 \text{ N/mm}^2$ , the material begins to plastically deform, that is, creeping of materials appears and the experimental results are considerably greater than the numerical results. Therefore, the value of  $\sigma_{\max} = 90 \text{ N/mm}^2$  has been chosen to define the limits of displacement condition. The used material model can only partially describe the real material behavior in the area of elastic and hyper-elastic deformation, but it cannot describe the real material behavior in the area of plastic deformation.

Due to the elastic segments' elasticity, R-Ch mechanisms with flexure hinges can achieve only minor displacements. In other words, they have restricted movement.

ANSYS software has been used to research mobility's limitations. The links are assumed to be made of piacryl with the above-mentioned material properties (Young's modulus  $E = 3700 \text{ N/mm}^2$ , flexural strength  $\sigma_{bs} = 90 \text{ N/mm}^2$ , the thickness of material  $\delta = 4 \text{ mm}$ ). The constraint positions of the links, in other words, the limits of angular displacement (mobility) and maximal bending force, have been determined by the condition  $\sigma_{\max} < \sigma_{bs}$ .

The results are shown in Table 2 as well as in Fig. 8.

Table 2  
Mobility of the R-ChCCMs with circular flexure hinges

<b>Mobility</b>		
<b>R-ChCCM</b>	<b>Input force case F<sub>a</sub></b>	<b>Input force case F<sub>b</sub></b>
First cognate (Fig. 3a)	$\Delta x_C = 10.98 \text{ mm}$	$\Delta x_C = 10.70 \text{ mm}$
	$\Delta y_C = 1.97 \text{ }\mu\text{m}$	$\Delta y_C = 6.1 \text{ }\mu\text{m}$
	$F_{\max} = 6.3 \text{ N}$	$F_{\max} = 10.7 \text{ N}$
Second cognate (Fig. 3c)	$\Delta x_C = 12.11 \text{ mm}$	$\Delta x_C = 12.01 \text{ mm}$
	$\Delta y_C = 10.81 \text{ }\mu\text{m}$	$\Delta y_C = 8.0 \text{ }\mu\text{m}$
	$F_{\max} = 6.4 \text{ N}$	$F_{\max} = 8.7 \text{ N}$

The best mobility (maximal constraint positions of the links) has been provided by the second R-ChCCM with circular flexure hinges, with the point of application of input load force located in the middle of the "input crank". However, this mobility is only 10% greater than the mobility of the first R-ChCCM with the point of application of input load force located in the middle of the "input crank". The first R-ChCCM with circular flexure hinges, with the point of application of input load force situated in the middle of the "input crank", has provided the highest guiding accuracy (minimum variation between absolute rectilinear and realized trace) of the "coupler" point on the rectilinear trace. This compliant mechanism produces much greater guiding accuracy than all other above-mentioned compliant mechanisms.

We have also analyzed the mobility of the first R-ChCCM with circular flexure hinges with double dimensions keeping the same rigidity ratio of 10: relatively rigid segments width  $w_R = 10 \text{ mm}$  and relatively elastic segments width  $w_E = 1 \text{ mm}$  in the first case, and  $w_R = 20 \text{ mm}$  and  $w_E = 2 \text{ mm}$  in the second case. The mobility is almost doubled ( $\Delta x_C = 21.4 \text{ mm}$  in comparison with  $\Delta x_C = 10.98 \text{ mm}$ ) with the maximal deviation  $\Delta y_C = 7.97 \text{ }\mu\text{m}$  in the first case and  $\Delta y_C = 6.36 \text{ }\mu\text{m}$  in the second case. However, let's compare the guiding accuracy on the same horizontal displacement of  $\Delta x_C = 10.98 \text{ mm}$ . The best result has been obtained for the first R-ChCCM with original dimensions:  $\Delta y_C = 1.97 \text{ }\mu\text{m} < 3.31 \text{ }\mu\text{m}$  (the second case of double scale-up mechanism)  $< 4.09 \text{ }\mu\text{m}$  (the first case of double scale-up mechanism).

We have analyzed the guiding accuracy and mobility of the first R-ChCCM with circular flexure hinges with the location of the point of application of force in the

middle of the "input crank" expecting that the point of application of force near the flexure hinge could cause the larger deformation of that joint with the influence to decrease the guiding accuracy of the coupler point. To confirm this assumption, we have also analyzed the guiding accuracy and mobility of the first R-ChCCM with circular flexure hinges, with different cases of the location of the point of application of force on the "input crank": the distance of the one-quarter of the length from the joint  $A_0$  (the first case), the distance of the one half of the length from the joint  $A_0$  (the middle of the "input crank" – the second case), the distance of the three-quarter of the length from the joint  $A_0$  (the third case), the distance of full the length from the joint  $A_0$  (the end of the "input crank" - the fourth case). We have obtained similar mobility in all cases – the maximal displacement  $\Delta x_C$  ranges from 10.884 mm to 11.029 mm. However, the best-guiding accuracy has been obtained for the location of the point of application of input load force in the middle of the "input crank – the second case:  $\Delta y_C = 1.97 \mu\text{m} < 2.87 \mu\text{m}$  (the fourth case of the location of the point of application of force)  $< 3.08 \mu\text{m}$  (the third case of the location of the point of application of force)  $< 4.62 \mu\text{m}$  (the first case of the location of the point of application of force).

## 5 The R-ChCCMs with Undercut Flexure Hinges

The undercut flexure hinges also fall into the group of circular flexure hinges. A circular notch and an undercut notch can look identical. The only difference is the asymmetry of these undercut flexure hinges (Fig. 5).

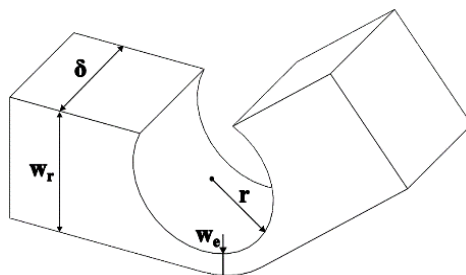


Figure 5

The design of the undercut flexure hinge

With the implementation of undercut flexure hinges in the design of the R-ChCCMs, a completely new model of this mechanism is obtained, which is shown in Fig. 6. As it can be seen in Fig. 6, the undercut flexure hinges are not put on the positions of joints  $A_0$  and  $B_0$  because they are used in areas where there are opportunities for authorized movement, which is essential in the ensuing optimization. If not, the mechanism's original design would be significantly altered.

The numerical simulations of such mechanisms were conducted in ANSYS using a 2D static structural analysis. As in the previous case discussed in Section 4, piacryl was used as the structural material and modeled as a linear, isotropic, and elastic material with constant values of Young's modulus ( $E = 3700 \text{ N/mm}^2$ ), flexural strength  $\sigma_{bs} = 90 \text{ N/mm}^2$  and the thickness of material  $\delta = 4 \text{ mm}$ . As shown in Figure 6, boundary conditions (fixed supports A and B) and loading scenarios (Forces A and B represented as C) were applied at predefined points on the input links.

To ensure accurate results, mesh refinement was employed. The global element size was set to 2 mm, while edge sizing was applied to the flexure hinge regions with a fine mesh of 0.1 mm to properly capture localized deformations. The mesh metric spectrum was evaluated, yielding a quality value of 0.81343, which indicates acceptable mesh integrity for structural simulations. No mesh convergence study was performed, as this mesh configuration showed numerically stable and physically consistent results.

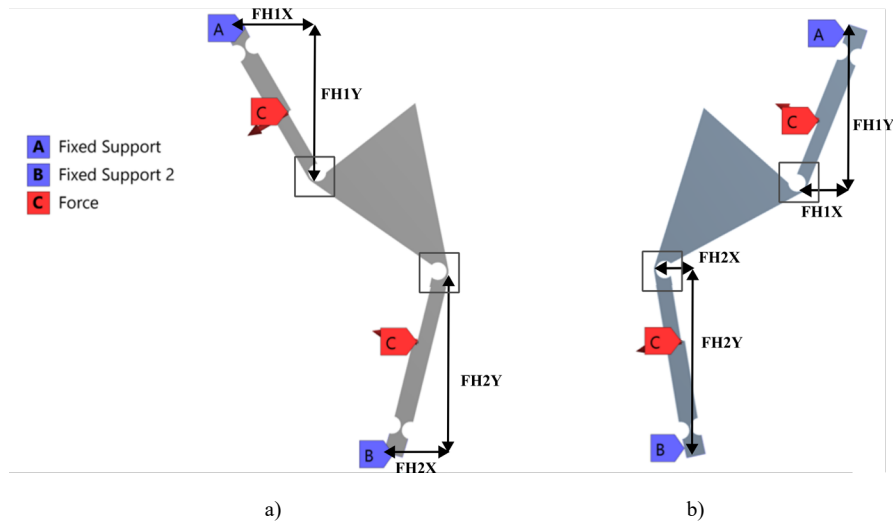


Figure 6

(a) The first R-ChCCM and (b) The second R-ChCCM with undercut flexure hinges, boundary conditions, and positional optimization input parameters

For improvement of a compliant mechanism based on a four-bar linkage design by the undercut flexure hinges in general comes down to a change in the position of these flexure hinges relative to the initially set position of joints. This is done using optimization tools. The displacement of the undercut flexure hinges, which was parameterized in both the X (shown in Fig. 6 as FH1X and FH2X for both R-ChCCM) and the Y (shown in Fig. 6 as FH1Y and FH2Y for both R-ChCCM) directions, will be the primary target of positional optimization.

## 6 Positional Optimization of Undercut Flexure Hinges

The goal of optimization is to establish the optimal location of the undercut flexure hinges to minimize the parasitic movement of the coupler point C ( $\Delta y_C$ ) along the rectilinear trace of  $\Delta x_C = 5$  mm. Therefore, the optimization process is formulated as a multi-objective problem, with the primary objective function being the minimization of the parasitic displacement  $\Delta y_C$ , while ensuring that  $\Delta x_C$  is above 5 mm. Additionally, two parameters (directional displacement  $\Delta x_C$  and  $\Delta y_C$ ) and maximal strain are observed as output in optimization. Maximal strain is used as a parameter ensuring that the resulting optimization mechanism remains within the elastic deformation range.

The design variables include the positions of the flexure hinges in both vertical and horizontal directions (parameters FH1X, FH1Y, FH2X, and FH2Y, as shown in Fig. 6). The ANSYS identifications of these parameters are represented by characters in parentheses. These variables, i.e., input parameters, are allowed to vary within predefined limits, represented by a grey rectangle in Fig. 6, where each mean value can change within a range of  $\pm 5$  mm from the nominal four-bar linkage joint position. This defines the minimum and maximum limits in positional optimization.

Tables 3 and 4 present the position value limits of the undercut flexure hinges in the R-ChCCM design. The positions of the first and second flexure hinges (P1 to P4) have minimum, mean, and maximum values that reflect the mechanism's adaptable nature. The boundary conditions, input forces A and B (P5), include a  $\pm 20\%$  difference from the mean force magnitude.

Table 3  
The first R-ChCCM inputs

		<i>Minimum</i>	<i>Mean Value</i>	<i>Maximal</i>
<b>Position of first flexure hinge (mm)</b>	<b>P1 - FH1X</b>	30.14	36	40.14
	<b>P2 - FH1Y</b>	75.92	81	85.92
<b>Position of second flexure hinge (mm)</b>	<b>P3 - FH2X</b>	19.34	24	29.34
	<b>P4 - FH2Y</b>	93.21	98	103.21
<b>P5 - Force A (N)</b>		1.32	1.65	1.98
<b>P5 - Force B (N)</b>		2.56	3.2	3.84

Table 4  
The second R-ChCCM inputs

		<i>Minimum</i>	<i>Mean Value</i>	<i>Maximal</i>
<b>Position of first flexure hinge (mm)</b>	<b>P1 - FH1X</b>	27.17	33	37.17
	<b>P2 - FH1Y</b>	76.93	81.5	86.93
<b>Position of second flexure hinge (mm)</b>	<b>P3 - FH2X</b>	11.78	16.5	21.78
	<b>P4 - FH2Y</b>	94.78	99.5	104.78

<b>P5 - Force A (N)</b>	1.24	1.55	1.86
<b>P5 - Force B (N)</b>	1.76	2.2	2.64

Tables 5 and 6 summarize the results of the positional optimization of the R-ChCCM with undercut flexure hinges. These results provide insights into the mechanism's behavior when subjected to distinct forces (Force A and Force B). The "Directional Deformation" (output parameters P6 and P7) highlights the position of coupler point C along specific axes, representing the parasitic movement  $\Delta y_C$  and the rectilinear trace of  $\Delta x_C$ . The "Equivalent Elastic Strain Maximum" (P8) values, expressed as percentages, indicate material deformation under applied forces. For Force A, this strain ranges from 0.729% to 1.489%, and for Force B, it spans from 0.4657% to 1.99% for the first R-ChCCM, while for the second R-ChCCM, it ranges from 0.821% to 1.443% for Force A and from 0.6555% to 1.702% for Force B.

A quadratic parameter determination matrix is obtained using sensitivity analysis. Fig. 7 provides an overview of key parameters, illustrating their influence. The quadratic matrices in Fig. 7 show parameter interdependencies with values ranging from 0 to 1 (from gray to red color). Although all input parameters are considered, only certain ones significantly affect rectilinear guidance error. For instance, parameters P1, P2, and P5 (location of the first undercut flexure hinge along the x and y axes and force, respectively) have a substantially greater impact on all output parameters than other input parameters.

Table 5  
The first R-ChCCM outputs

		<i>Calculated Minimum</i>	<i>Calculated Maximum</i>
<b>P6 - Directional Deformation</b> <b><math>\Delta x_C</math> (mm)</b>	Force A (N)	-7.17788	-3.08619
	Force B (N)	-9.6379	-1.9016
<b>P7 - Directional Deformation</b> <b><math>\Delta y_C</math> (mm)</b>	Force A (N)	-0.34887	0.33099
	Force B (N)	-0.2669	0.43071
<b>P8 - Equivalent Elastic Strain</b> <b>Maximum (%)</b>	Force A (N)	0.729	1.489
	Force B (N)	0.4657	1.99

Table 6  
The second R-ChCCM outputs

		<i>Calculated Minimum</i>	<i>Calculated Maximum</i>
<b>P6 - Directional Deformation</b> <b><math>\Delta x_C</math> (mm)</b>	Force A (N)	-7.1727	-3.3479
	Force B (N)	-8.0882	-2.807
<b>P7 - Directional Deformation</b> <b><math>\Delta y_C</math> (mm)</b>	Force A (N)	-0.3594	0.2372
	Force B (N)	-0.40578	0.2167
<b>P8 - Equivalent Elastic Strain</b> <b>Maximum (%)</b>	Force A (N)	0.821	1.443
	Force B (N)	0.6555	1.702

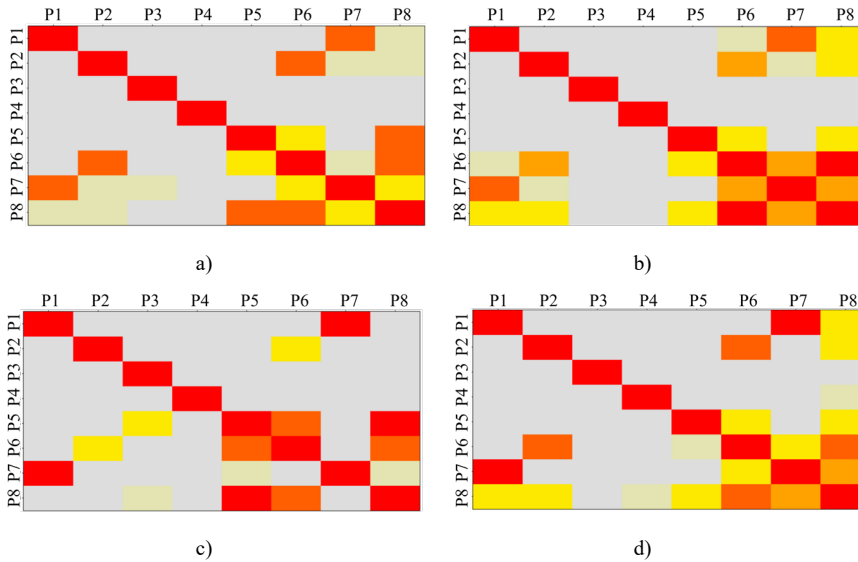


Figure 7

Obtained quadratic determination matrix for the case of the first R-ChCCM for applied force A (a) force B (b) and the second R-ChCCM for applied force A (c) and force B (d) (input parameters from P1 to P5 and output parameters from P6 to P8)

The positional optimization was conducted using a multi-objective genetic algorithm (MOGA), where the best solution was selected from the Pareto optimal set [35]. The optimization objectives and constraints were defined such that the displacement of point C in the X direction ( $\Delta x_C$ ) had to be greater than 5 mm, while the parasitic displacement  $\Delta y_C$  was minimized to approach 0 mm.

Four separate positional optimizations were conducted, yielding three sets of dimensions (candidate points) for each optimization. The input parameters for candidates with the best results are shown in Table 7.

Table 7  
The R-ChCCM obtained positional optimization inputs

		The first R-ChCCM		The second R-ChCCM	
		Input force case $F_a$	Input force case $F_b$	Input force case $F_a$	Input force case $F_b$
Position of first flexure hinge (mm)	P1 - FH1X	36.02348567	37.00632471	33.197	32.59804115
	P2 - FH1Y	81.61680078	83.36973047	83.32993	81.73557
Position of second flexure hinge (mm)	P3 - FH2X	21.91555436	22.46095123	17.75417	15.15337
	P4 - FH2Y	96.40605497	99.1204809	101.6578	96.61916

This positional optimization has been also used to determine the mobility of the R-ChCCMs with undercut flexure hinges taking into consideration flexural strength  $\sigma_{bs} = 90 \text{ N/mm}^2$  and condition  $\sigma_{max} < \sigma_{bs}$ , as it has already been done for the compliant mechanisms with circular flexure hinges, but without the positional optimization (section 4).

The results of positional optimization have been shown in Table 8, as well as in Fig. 8.

Table 8  
Mobility of the R-ChCCMs with undercut flexure hinges

Mobility		
R-ChCCM	Input force case $F_a$	Input force case $F_b$
First cognate (Fig. 6a)	$\Delta x_C = 11.008 \text{ mm}$	$\Delta x_C = 11.785 \text{ mm}$
	$\Delta y_C = 0.55942 \text{ }\mu\text{m}$	$\Delta y_C = 0.58699 \text{ }\mu\text{m}$
	$F_{max} = 3.593 \text{ N}$	$F_{max} = 6.76 \text{ N}$
Second cognate (Fig. 6b)	$\Delta x_C = 11.186 \text{ mm}$	$\Delta x_C = 10.838 \text{ mm}$
	$\Delta y_C = 0.22503 \text{ }\mu\text{m}$	$\Delta y_C = 0.11699 \text{ }\mu\text{m}$
	$F_{max} = 3.261 \text{ N}$	$F_{max} = 4.835 \text{ N}$

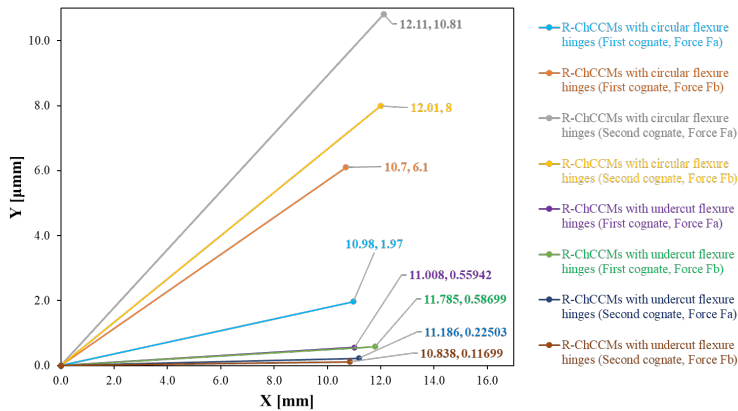


Figure 8  
Mobility graph of the R-ChCCMs obtained from Table 2 and Table 8

The effectiveness of the optimization is evident in the achieved reduction of parasitic displacement  $\Delta y_C$ . These results, shown in Table 9, demonstrate a significant improvement in minimizing parasitic displacement, validating the effectiveness of the optimization approach.

Table 9  
Positional optimization results summary

	$\Delta y_C$ Before Optimization ( $\mu\text{m}$ )	$\Delta y_C$ After Optimization ( $\mu\text{m}$ )	Improvement (%)
<b>First R-ChCCM, Force A</b>	43.19	0.55942	98.7
<b>First R-ChCCM, Force B</b>	46.239	0.58699	98.73
<b>Second R-ChCCM, Force A</b>	36.445	0.22503	99.38
<b>Second R-ChCCM, Force B</b>	35.311	0.11699	99.67

Maximum equivalent elastic strain is used as a constraint instead of stress (which was used in section 4), due to its practical suitability. Since the relationship between strain and stress in the elastic deformation range follows the linear relationship defined by Hooke's law, the equivalent elastic strain provides a direct means of controlling stress levels in the design process. This is confirmed and illustrated in Figure 9, using the example of the second R-ChCCM with force  $F_b$ , which yielded the most accurate guiding performance.

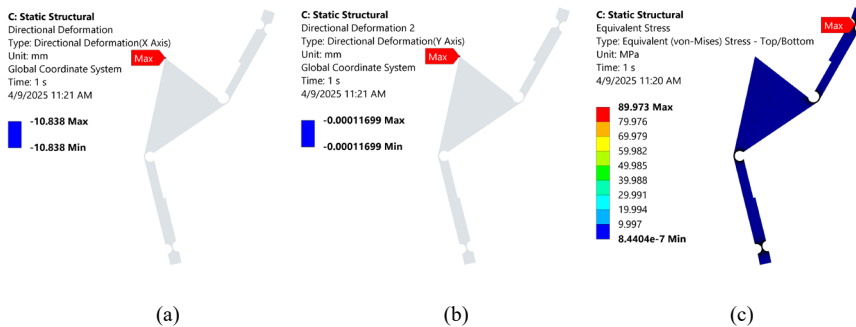


Figure 9

Obtained results for the second R-ChCCM with input force  $F_b$ : (a) The rectilinear trace ( $\Delta x_C$ ), (b) The parasitic movement of the coupler point C ( $\Delta y_C$ ), (c) Maximal stress

## Conclusions

The frequent synthesis method for the compliant mechanism, is to design it as the counterpart of the rigid-body linkage, which can realize the pre-defined function (rigid-body replacement method). This paper has introduced the design of the cognate-compliant four-bar linkages. The two cognate-compliant mechanisms (CCMs) have been developed as counterparts of the rigid-body Roberts–Chebyshev (R–Ch) mechanism, where the coupler point coupler point C, which is situated in the coupler's corner (Fig. 1), can be directed on an approximate rectilinear trace. The CCMs with circular flexure hinges as well as with undercut flexure hinges have been analyzed. It has been shown that Roberts–Chebyshev theorem, concerning a coupler curve being generated by three different four-bar linkages, should be also applied on the compliant mechanism.

The guiding accuracy, that is, the difference between realized and exact rectilinear trace, as well as the mobility, that is, determining the constraint position of the links, have been analyzed and compared for all above-mentioned compliant mechanisms being suitable to realize approximate rectilinear guiding of the coupler point.

The first Roberts–Chebyshev cognate-compliant mechanism (R-ChCCM) with circular flexure hinges, with the point of application of input load force situated in the middle of the "input crank", has provided the highest guiding accuracy (minimum variation between absolute rectilinear and realized trace) of the "coupler" point on the rectilinear trace.

Alternatively, the best mobility (maximal constraint positions of the links) has been provided by the second R-ChCCM with circular flexure hinges, with the point of application of input load force located in the middle of the "input crank". However, this mobility is only 10% greater than the mobility of the first R-ChCCM with the point of application of input load force located in the middle of the "input crank".

Introducing the undercut flexure hinges and their positional optimization has improved the guiding accuracy as well as the mobility of the R-ChCCMs.

The second R-ChCCM with undercut flexure hinges, with the point of application of input load force situated in the middle of the "follower", has provided the highest guiding accuracy.

Conversely, the best mobility has been provided by the first R-ChCCM with undercut flexure hinges, with the point of application of input load force located in the middle of the "follower". However, this mobility is only 9% greater than the mobility of the second R-ChCCM with undercut flexure hinges, with the point of application of input load force situated in the middle of the "follower".

The second R-ChCCM with undercut flexure hinges, with the point of application of input load force situated in the middle of the "follower" produces much greater guiding accuracy than all other above-mentioned compliant mechanisms. This guiding accuracy is even better than the theoretical rectilinear guiding accuracy of the rigid-body counterpart linkage. It should be mentioned that the production of rigid-body linkages is not possible without appearing of the tolerance of the link lengths and clearance in the revolute joints, which decreases the guiding accuracy. This compliant mechanism, therefore, is to be suggested for realizing rectilinear guiding of the "coupler" point.

The cognate compliant mechanism has realized a smaller deviation between exact rectilinear and realized path than the basic compliant mechanism, and this fact confirms our suggestion that the results of guiding accuracy, as well as mobility offered by the cognate compliant mechanisms, should be taken into consideration in the synthesis procedure of the compliant mechanisms.

Although the primary focus of this paper is the position optimization of the Roberts–Chebyshev cognate mechanisms, the long-term reliability of compliant mechanisms under cyclic loading remains a critical aspect for future investigation. Several studies have addressed fatigue behavior in flexure hinges and compliant structures [37-41]. These works underline the importance of geometry-specific fatigue behavior in compliant mechanisms, which will be the focus of future studies aiming to improve the durability of Roberts–Chebyshev type compliant mechanisms under periodic loading.

### Acknowledgment

This research was financially supported by the Ministry of Education, Science and Technological Development of the Republic of Serbia (Contract No. 451-03-136/2025-03/ 200109).

### References

- [1] Aboulissane, B., El Bakkali, L., El Bahaoui, J. (2020) Workspace analysis and optimization of the parallel robots based on computer-aided design approach, *Facta Universitatis, Series Mechanical Engineering* 18(1):079-089
- [2] Aboulissane, B., El Haiek, D., El Bakkali, L., El Bahaoui, J. (2019) On the workspace optimization of parallel robots based on CAD approach, *Procedia Manufacturing* 32:1085-1092
- [3] Yang, Z. G., Shao, M. L., Shin, D. I. (2015) Kinematic optimization of parallel manipulators with a desired workspace, In *Applied Mechanics and Materials*, Trans Tech Publications Ltd 752:973-979
- [4] Tsirogiannis, E., Vosniakos, G. (2019) Redesign and topology optimization of an industrial robot link for additive manufacturing, *Facta Universitatis, Series Mechanical Engineering* 17(3):415-424
- [5] Junk, S., Klerch, B., Nasdala, L., Hochberg, U. (2018) Topology optimization for additive manufacturing using a component of a humanoid robot, *Procedia Cirp* 70:102-107
- [6] Fetisov, K. V., Maksimov, P. V. (2018) Topology optimization and laser additive manufacturing in the design process of efficiency lightweight aerospace parts, In *Journal of Physics: Conference Series*, IOP Publishing 1015 (5):052006
- [7] Habashneh, M., Rad, M. M., & Fischer, S. (2023) Bi-directional Evolutionary, Reliability-based, Geometrically Nonlinear, Elasto-Plastic Topology Optimization, of 3D Structures. *Acta Polytechnica Hungarica*, 20(1)
- [8] Fragassa, C. (2021) Lightening structures by metal replacement: from traditional gym equipment to an advanced fiber-reinforced composite exoskeleton, *Facta Universitatis, Series Mechanical Engineering*:155-174

- [9] Both, J., Morasch, A., Wehrle, E., Baier, H. (2011) Advanced manufacturing and design techniques for lightweight structures, *International Aluminium Journal* 87:60-64
- [10] Heggemann, T., Homberg, W. (2019) Deep drawing of fiber metal laminates for automotive lightweight structures, *Composite Structures* 216:53-57
- [11] Zentner, L., Linß, S. (2019) *Compliant systems - Mechanics of elastically deformable mechanisms, actuators and sensors*, De Gruyter, Oldenbourg, Muenchen
- [12] Chrysilla, G., Eusman, N., Deguet, A., & Kazanzides, P. (2019) A compliance model to improve the accuracy of the da Vinci Research Kit (dVRK) *Acta Polytechnica Hungarica*, 16(8)
- [13] Howell, L. L., Magleby, S. P., Olsen, B. M. (2013) *Handbook of Compliant Mechanisms*, John Wiley & Sons Inc., New York
- [14] Howell, L. L. (2001) *Compliant mechanisms*, John Wiley & Sons, Inc., NY
- [15] Midha, A., Norton, T. W., Howell, L. L. (1994) On the nomenclature, classification, and abstractions of compliant mechanisms, *ASME Journal of Mechanical Design* 116 (1):270-279
- [16] Howell, L. L., Midha, A. (1994) Method for the design of compliant mechanisms with small-length flexural pivots, *ASME Journal of Mechanical Design* 116 (1):280-290
- [17] Ananthasuresh, G. K., Kota, S. (1995) Designing compliant mechanisms, *Mechanical Engineering* 117 (11): 93-96
- [18] Böttcher, F., Christen, G., Pfefferkorn, H. (2001) Structure and function of joints and compliant mechanism, *Motion Systems (Collected Short Papers of the Innovationskolleg "Bewegungssysteme" Friedrich-Schiller Universität Jena)*, TU Jena, TU Ilmenau, ShakerVerlag, Aachen: 30-35
- [19] Pavlović, N. D., Pavlović, N. T. (2013) *Compliant mechanisms (in Serbian)*, Faculty of Mechanical Engineering, University of Niš, Serbia
- [20] Pavlović, N. T., Pavlović, N. D. (2003) Motion characteristics of the compliant four-bar linkages for rectilinear guiding, *Journal of Mechanical Engineering Design (Yugoslav Society for Machine Elements and Design)* 6 (1):20-27
- [21] Pavlović, N. T., Pavlović, N. D. (2004) Rectilinear guiding accuracy of Roberts-Chebyshev compliant four-bar linkage with silicone joints, *Mehanika na mašinice* 12 (4):53-56
- [22] Pavlović, N. T., Pavlović, N. D., Milošević, M. (2016) Selection of the optimal rigid-body counterpart mechanism in the compliant mechanism

- synthesis procedure, Microactuator and Micromechanisms, Proceedings of MAAM, Ilmenau, Germany, October 5-7, 2016, Springer:127-138
- [23] Pavlović, N. T., Pavlović, N. D. (2009) Compliant mechanism design for realizing of axial link translation, *Mech and Mach. Theory* 44(5):1082-1091
- [24] Pavlović, N. T., Stojiljković, D. (2022) Guiding accuracy of the Watt compliant cognate mechanisms, *Facta Universitatis, Series: Mechanical Engineering*, <https://doi.org/10.22190/FUME220822044P>, Preprint at <http://casopisi.junis.ni.ac.rs/index.php/FUMechEng/article/view/11038>
- [25] Yuan, Y., Ren, J., Wang, Z., Mu, X. (2022) Dynamic analysis of the rigid-flexible excavator mechanism based on virtual prototype, *Facta Universitatis, Series: Mechanical Engineering* 20(2):341-361
- [26] Ling, M., Cao, J., Howell, L. L., Zeng, M. (2018) Kinetostatic modeling of complex compliant mechanisms with serial-parallel substructures: A semi-analytical matrix displacement method, *Mechanism and Machine Theory*, S0094114X17317718–
- [27] Dao, T., Huang, S. C. (2017) Optimization of a two degrees of freedom compliant mechanism using Taguchi method-based grey relational analysis, *Microsystem Technologies*, doi:10.1007/s00542-017-3292-1
- [28] Dunning, A. G., Tolou, N., Pluimers, P. P., Kluit, L. F., Herder, J. L. (2012) Bistable Compliant Mechanisms: Corrected Finite Element Modeling for Stiffness Tuning and Preloading Incorporation, *ASME. J. Mech. Des.* August 2012; 134(8): 084502
- [29] Chia, N. W. *et al* (2019) Optimization on effects of design parameter on displacement amplification ratio of 2 DOF working platform employing Bridge-type compliant mechanism flexure hinge using Taguchi method, *J. Phys.: Conf. Ser.* 1303012053
- [30] Patil, V. S., Anerao, P. R., Chinchankar, S. S. (2018) Design and Analysis of Compliant Mechanical Amplifier, *Materials Today: Proceedings* 5, No. 5 (2018): 12409-12418
- [31] Parag, M. *et al* (2021) Development of Bridge and Lever Type Compact Compliant Mechanism for Micro Positioning Systems, *J. Phys.: Conf. Ser.* 1969 012006
- [32] Hao, G., Li, H., He, X., Kong, X. (2014) Conceptual design of compliant translational joints for high-precision applications, *Front. Mech. Eng.* 9(4): 331-343
- [33] Pavlović, N. T., Pavlović, N. D. (2018) Design of Compliant Cognate Mechanisms, *Proceedings of the 4<sup>th</sup> Int. Conference "Mechanical Engineering in XXI Century"*, Niš, Serbia: 253-258

- [34] Pavlović, N. T, Pavlović, N. D. (2005) Mobility of the flexure hinges and compliant mechanisms, *Theoretical and Applied Mechanics*, Belgrade 32 (4):341-357
- [35] Čabala, J., & Jadlovský, J. (2020) Choosing the optimal production strategy by multi-objective optimization methods. *Acta Polytechnica Hungarica*, 17(5), 7-25
- [36] Pavlović, N. T., Christen, G. (2002) Experimental Research of The Compliant Four-Bar Linkage for Rectilinear Guiding, 47<sup>th</sup> Internationales Wissenschaftliches Kolloquium, Proceedings, pp. 320-321, CD, TU Ilmenau
- [37] Schoenen, J., Hüsing, P., Corves, B. (2016) Dynamic Analysis of a Fatigue Test Bench for High-Precision Flexure Hinges, In: *Advances in Service and Industrial Robotics, Mechanisms and Machine Science*, Vol. 40, Springer, pp. 175-183
- [38] Tawk, C., Goldsmith, C., Armand, M., and Tholey, G. (2018) Modelling and Verification of Fatigue Damage for Compliant Mechanisms, *Robotica*, 37(1), pp. 174-195
- [39] Ivanov, I., Corves, B. (2014) Fatigue Testing of Flexure Hinges for High-Precision Micro Manipulators, *Mechanical Sciences*, 5, pp. 59-64
- [40] Stasiulevičius, J., Bogušis, V., Grinkevičius, L., Šešok, D. (2020) Compliance and Fatigue Life Analysis of U-shaped Flexure Hinge, *Mechanika*, 26(3), pp. 202-208
- [41] Su, H., McCarthy, S. P., Midha, A. (2015) Fatigue Evaluation and Performance Optimization of Flexure-Based Compliant Mechanisms, *Mechanism and Machine Theory*, 90, pp. 34-50